Laser Magnetic Resonance Spectroscopy of ClO and Kinetic Studies of the Reactions of ClO with NO and NO$_2$

YUAN-PERN LEE,* RICHARD M. STIMPFLE,[t‡] ROBERT A. PERRY,** JOHN A. MUCHA,[§] KENNETH M. EVENSON,[°] DONALD A. JENNINGS,[°] and CARLETON J. HOWARD[t]

Aeronomy Laboratory, NOAA Environmental Research Laboratory, Boulder, Colorado 80303

Abstract

Far-infrared rotational transitions in ClO(X$^2\Pi_{3/2}$, v = 0) have been observed using laser magnetic resonance (LMR) with an optically pumped spectrometer. Five observed transitions at wavelengths between 444 and 713 μm have been compared with values predicted with spectroscopic constants from the literature. LMR detection of ClO has been used to study its reactions with NO and NO$_2$ in a discharge flow system under pseudo-first-order conditions for ClO. The measured rate constants are k(ClO + NO) = (7.1 ± 1.4) × 10^{-12} exp[(270 ± 50)/T] cm^3/molec·s for the temperature range of 202 < T < 393 K; k(ClO + NO$_2$ + M) = (2.8 ± 0.6) × 10^{-33} exp[(1090 ± 80)/T] cm^6/molec^2·s (M = He, 250 < T < 387 K), (3.5 ± 0.6) × 10^{-33} exp[(1180 ± 80)/T] (M = O$_2$, 250 < T < 416 K), and (2.09 ± 0.3) × 10^{-31} (M = N$_2$, T = 297 K). All measurements were made at low pressures, between 0.6 and 6.6 torr. These results are compared with those from other studies.

Introduction

The potential impact of stratospheric ozone depletion by the chlorine catalytic cycle

(1) $$Cl + O_3 \rightarrow ClO + O_2$$

(2) $$\underline{ClO + O \rightarrow Cl + O_2}$$

$$Net: \ O_3 + O \rightarrow 2O_2$$
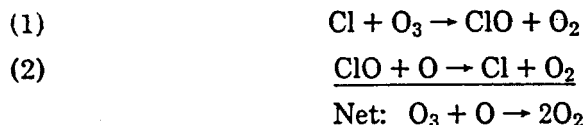
* NOAA-CIRES Postdoctoral Research Associate. Present address: Chemistry Department, National Tsing-Hua University, Hsin-Chu, Taiwan, Republic of China.
[t] Also affiliated with the Department of Chemistry, University of Colorado, Boulder, CO 80309.
[‡] Present address: Division of Applied Sciences, Harvard University, Cambridge, MA 02138.
** NOAA-NRC Postdoctoral Research Associate. Present address: Combustion Research Facility, Sandia Laboratories, Livermore, CA 94550.
[§] NBS-NRC Postdoctoral Research Associate. Present address: Bell Laboratories, Murray Hill, NJ 07974.
[°] National Bureau of Standards, Time and Frequency Division, Boulder, CO 80303.

has generated considerable interest [1]. To evaluate the effects of chlorine on ozone one must consider the reactions involving the active species Cl and ClO. The presence of nitrogen oxides (NO and NO_2) in the stratosphere limit the effectiveness of the chlorine cycle. First, the reaction with NO,

(3) $ClO + NO \rightarrow Cl + NO_2$

when combined with

(4) $NO_2 + h\nu(\lambda < 380 \text{ nm}) \rightarrow NO + O$

(5) $O + O_2 + M \rightarrow O_3 + M$
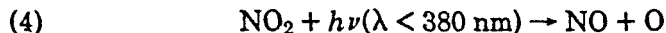
and reaction (1) produces no net destruction of ozone. Second, the reaction of ClO with NO_2,

(6) $ClO + NO_2 + M \rightarrow ClNO_3 + M$

forms $ClNO_3$ [2], which is thought to be an unreactive reservoir for chlorine.

There have been five studies of the ClO + NO reaction. Clyne and Watson [3] first measured the rate constant $k = (1.7 \pm 0.2) \times 10^{-11}$ cm³/ molec·s at room temperature using discharge-flow/mass spectrometry in 1974. Later Zahniser and Kaufman [4] employed the discharge-flow/ resonance fluorescence technique to determine the rate constant relative to that of the Cl + O_3 reaction. They reported rate constants at temperatures ranging from 230 to 295 K, giving a room temperature value slightly higher than the previous value and a negative Arrhenius activation energy of 400 cal/mol (1 cal = 4.184 J). Leu and DeMore [5] investigated the temperature dependence (227–415 K) using mass spectrometry and obtained slightly lower rate constants and a negative activation energy of about 590 cal/mol. Recently Clyne and MacRobert [6] and Ray and Watson [7] repeated the measurement at room temperature and reported rate constants close to the first study.

The ClO + NO_2 + M reaction in the low-pressure range of 1–6 torr (1 torr = 133.3 Pa) has been studied by three groups [8–10] using discharge-flow techniques with various detection methods. Leu et al. [8] and Birks et al. [9] detected ClO by mass spectrometry. This technique was complicated by effects of $ClNO_3$ fragmentation in the mass spectrometer ion source to produce ClO. Since the rate constant measurement is based on the pseudo-first-order decay of ClO, this effect could lead to an underestimation of the true value of k_6. Birks et al. used an empirically derived correction for this effect that increased the measured value by up to about 17%, while Leu et al. operated under conditions which they stated required no correction. Zahniser et al. [10] detected ClO indirectly by conversion of ClO to Cl with NO addition, reaction (3), followed by resonance fluorescence detection of the Cl atoms.

While the various rate constant measurements for both reactions (3) and (6) are in reasonable agreement, some significant discrepancies still exist. For the ClO + NO reaction, the rate constants given by the two temperature dependence studies [4,5] differ by about 40%. For the ClO + NO_2 + M reaction the reported rate constants at room temperature differ by about 30% in He and by about 20% in N_2. In addition, the reaction

(7) $$ClO + O_2 + M \rightarrow OClO_2 + M$$
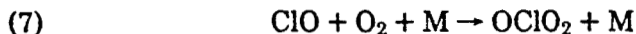
may take place at high O_2 concentrations and could have an effect on the ClO + NO_2 + O_2 reaction. Since no measurements of k_6 were made in O_2, it is interesting to investigate reaction (6) in O_2 as a first step toward the understanding of the importance of reaction (7) and the chemistry of $OClO_2$ in the stratosphere. Also it is worthwhile to test a new method which detects ClO directly, has high sensitivity, and does not have possible complications from the product $ClNO_3$ or other species.

Here we report the far-infrared (FIR) laser magnetic resonance (LMR) spectra of ClO at five different laser frequencies. Applying this LMR detection technique, we have also investigated the temperature dependence of the rate constants of reactions (3) and (6).

Experimental

An LMR spectrometer was used in conjunction with a discharge-flow tube in this study. The basic principles of LMR for spectroscopic as well as kinetic studies have been described previously [11,12]. Briefly, a continuous-wave CO_2 laser with an output power of approximately 25 W was used to pump a FIR CH_3OH, CD_3I, or DCOOH laser which produces about 100 μW. The intracavity absorption was accomplished by Zeeman tuning a rotational transition of the ClO molecule into resonance with the FIR laser frequency. The magnetic field can be varied up to 21 kG. High sensitivity was obtained by ac modulating the magnetic field and using frequency-locked phase-sensitive detection. It has been found that the peak-to-peak height of the first derivative of the absorption curve is proportional to the radical concentration [11].

In the kinetic studies, the rate constants were measured by observing the pseudo-first-order decay of ClO concentrations in a large excess of NO or NO_2 as a function of reaction time. The ClO radical was detected at $\simeq 0.5$ kG using a π-polarized 556.9-μm CD_3I laser line pumped by the 10P(36) CO_2 laser emission. The detection limit for ClO is approximately 2×10^8 molec/cm^3 (signal-to-noise ratio $\simeq 1$ at 1 s time constant).

The discharge-flow apparatus [12] consists of a 2.54-cm inside diameter, 110-cm long Pyrex flow tube with a 9-mm outside diameter movable inlet. The flow tube was mounted in the LMR spectrometer with the tube exit positioned directly above the intersection of the FIR laser beam and the magnetic field.

The total gas flow consisted of the carrier gas (He, O_2, or N_2), NO_2 or NO, and the gas mixture from the ClO source. For the ClO + NO_2 + M reaction rate measurements, the ClO source was part of the movable inlet which allowed variation of the position of the ClO injection into the flow tube. The ClO radical was formed by reacting Cl atoms with excess of O_3 in the top part of the movable inlet

(1) $Cl + O_3 \rightarrow ClO + O_2$

The Cl was generated by passing a trace of $Cl_2 \simeq 0.002$ STP cm^3/s (STP = 273 K, 1 atom) in helium carrier gas (0.2–0.4 STP cm^3/s) through a 20–35-W microwave discharge. Ozone was eluted with helium from a 196 K silica gel trap and diluted with additional helium (0.3–1.0 STP cm^3/s) before reacting with Cl atoms. The ClO formation is >99% completed within the first 5-cm length of injector based on the reported value [13] of $k_1 = 1.1 \times 10^{-11}$ cm^3/molec·s and the ozone concentration of about 3×10^{14} molec/cm^3. The distance from the O_3 inlet to the end of the injector was about 125 cm, long enough for any vibrationally excited ClO formed by reaction (1) to be quenched before it entered the reaction region. The ClO concentration in these experiments was about $(1–8) \times 10^{12}$ molec/cm^3. At this concentration ClO does not react significantly with itself in the flow tube [13].

For the ClO + NO_2 + M study, NO_2 was admitted into the flow tube through a side arm about 80 cm upstream of the LMR detection region. The NO_2 concentration in the flow tube ranged from 2 to 20×10^{14} molec/cm^3. The NO_2 flow rate was measured by observing the rate of the pressure change in a calibrated volume. The effect of NO_2 dimerization has been taken into account in the NO_2 flow rate measurements by applying the correction $F_{NO_2} = F'_{NO_2}(1 + 2\overline{P}/K_p)$, where F'_{NO_2} is the measured apparent NO_2 flow rate, $\overline{P}$ (in torr) is the average pressure in the calibrated volume, and $K_p = [NO_2]^2/[N_2O_4]$ is the equilibrium constant (in torr) for the NO_2 dimerization reaction. At 298 K, $K_p = 106$ torr [14], and the NO_2 flow-rate correction is less than 5% with $\overline{P} \simeq 2$ torr. NO_2 flow measurements were always made at low pressure to minimize the correction. The effect of NO_2 dimerization in the flow tube was negligible (<1%) at temperatures above 270 K for $[NO_2] < 2 \times 10^{15}$ molec/cm^3 ($K_p \simeq 9.7$ torr at 270 K).[1] However, at 250 K K_p decreased to 1.18 torr [15], and about a 4% decrease in NO_2 concentration due to dimerization should be taken into account for $[NO_2] \simeq 1 \times 10^{15}$ molec/cm^3.

For the ClO + NO reaction, the ClO was formed in the flow tube by reacting ozone, $(3–12) \times 10^{11}$ molec/cm^3, with excess Cl atoms, $(8–15) \times 10^{13}$ atom/cm^3, which were produced by a microwave discharge of Cl_2 and He in a sidearm of the flow tube. NO was mixed with ~0.5 STP cm^3/s of helium and added through the movable injector. The NO concentration in the flow tube ranged from $(3$ to $30) \times 10^{12}$ molec/cm^3.

---

[1] Obtained using thermochemical data from [15].

The carrier gas was added about 85 cm upstream of the LMR detection region with a flow rate between 2 and 30 STP cm³/s, depending on the desired flow velocity and pressure. The flow rates were measured with mass flowmeters which are accurate within ±3% [12]. The flow tube pressure was measured at the center of the reaction region with a capacitance manometer with an accuracy of about ±1% [12]. The flow tube pressure P_t ranged from 0.6 to 6.6 torr with the average flow velocity $\bar{v}$ ranging from 350 to 1000 cm/s for the ClO + NO₂ + M kinetic studies, while P_t = 1–3 torr and $\bar{v}$ = 1670–2730 cm/s for the ClO + NO studies.

Temperature variability of the flow tube from 202 to 416 K was achieved by circulating either liquid N₂, cooled ethanol, or heated dibutylphthalate through the flow tube jacket. The temperature of the circulating fluid was measured with a Pt resistance thermometer at the exit of the jacket, and it was shown previously that the temperature of the flow tube was uniform to ±1°C [12].

The He (>99.9996%, analyzed) was passed through a liquid N₂-cooled molecular sieve trap before use. O₂ and N₂ (>99.97%) and Cl₂ (>99.96%) were used without further purification. NO reactant was passed through a dry-ice–ethanol-cooled silica gel trap to remove other nitrogen oxides. NO₂ was synthesized by reacting purified NO (>99.0%) with excess of O₂, and stored under about 2 atm of O₂ for at least 24 h before use. During the kinetic measurements, the pure NO₂ (NO < 0.01%) was kept in an ice-water bath to maintain a constant pressure of ∼260 torr.

O₃ was prepared by passing O₂ through an ac discharge and collected in a silica gel trap kept in a dry-ice–ethanol bath. The ozone partial pressure P_{O_3} was measured by passing He–O₃ mixtures through a 10-cm absorption cell using 1.15×10^{-17} cm² as the O₃ absorption cross section at 254 nm [16]. Thus the flow rate of O₃, F_{O_3}, was calculated from the flow rate of He through the cell F_{He}, the total pressure in the cell P_A, and P_{O_3}:

$$(8) \qquad F_{O_3} = F_{He} P_{O_3}/(P_A - P_{O_3})$$

The estimated random error in a rate constant measurement is about 8%. This is based on the equation $k \propto F_T^2 T^3$ (slope)$/P_t^3 F_R r^2$ and the estimates of 3% error in flow rate measurements F_T and F_R, 1% in temperature T, 2% in the decay plot slope, 1% in pressure P_t, and 1% in the tube radius r. However, in consideration of possible systematic errors, ±15% is a more realistic estimate of the overall accuracy of the kinetic measurements.

ClO Spectroscopy

The LMR detection of a paramagnetic radical requires a close coincidence of an FIR laser frequency with a zero-field rotational transition, because the energy range over which a molecular rotational transition can be magnetically tuned is usually less than 1 cm⁻¹ for magnetic fields of less

than 20 kG (10^4 G = 1 T). In the case of ClO, the search for proper FIR laser frequencies that can yield LMR spectra is simplified because the molecular parameters for the ground state have been accurately determined [17–23]. Using the energy expression $E_J = B(J + \frac{1}{2})^2 - D(J + \frac{1}{2})^4$ from the analysis of Kakar et al. [17] and the values of $B = 0.61976$ cm^{-1}, $D = 1.315 \times 10^{-6}$ cm^{-1} for ^{35}ClO, and $B = 0.60930$ cm^{-1}, $D = 1.278 \times 10^{-6}$ cm^{-1} for ^{37}ClO, the zero-field rotational transition energies of ClO can be esti- mated with sufficient accuracy to predict near resonances. Listed in Table I are the estimated energies for the $\Delta J = +1$ rotational transitions of the ground $^2\Pi_{3/2}$ ($v = 0$) state of ^{35}ClO and ^{37}ClO.

The magnetic tunability of a rotational transition can be estimated from the first-order Zeeman interaction energy

(9) $$E_J = -g_J M_J \mu_B H$$

where g_J is the rotational g factor, μ_B is the Bohr magneton, M_J is the component of J in the field direction, and H is the magnetic field strength. The g_J factor for ClO may be approximated by [24]

(10) $$g_J \cong \frac{(\Lambda + \Sigma)(\Lambda + 2\Sigma)}{J(J + 1)}$$

where J is the total angular momentum quantum number, Λ is the orbital angular momentum projection quantum number, and Σ is the spin angular momentum projection quantum number. Thus of the two components

TABLE I. Estimated energies and vacuum wavelengths for $\Delta J = +1$ rotational transitions of the ground $^2\Pi_{3/2}$ ($v = 0$) state of ^{37}ClO and ^{35}ClO.

J″ (lower level)	^{37}ClO		^{35}ClO	
	E (cm^{-1})	λ(μm)	E (cm^{-1})	λ(μm)
1.5	3.046	3283	3.099	3227
2.5	4.265	2345	4.338	2305
3.5	5.483	1824	5.577	1793
4.5	6.701	1492	6.816	1467
5.5	7.919	1263	8.055	1241
6.5	9.137	1094	9.294	1076
7.5	10.35	965.7	10.53	949.4
8.5	11.57	864.1	11.77	849.5
9.5	12.79	781.9	13.01	768.7
10.5	14.01	714.0	14.25	701.9
11.5	15.22	656.9	15.48	645.8
12.5	16.44	608.3	16.72	598.1
13.5	17.65	566.4	17.96	556.9
14.5	18.87	530.0	19.19	521.0
15.5	20.08	497.9	20.43	489.5
16.5	21.30	469.5	21.66	461.6
17.5	22.51	444.2	22.90	436.7
18.5	23.72	421.5	24.13	414.4
19.5	24.92	401.0	25.36	394.2
20.5	26.15	382.4	26.60	376.0

of the $^2\Pi$ ClO ground electronic state, the $^2\Pi_{1/2}$ levels are not Zeeman active (because $\Lambda = \pm 1, \Sigma = \mp 1/2$), while the $^2\Pi_{3/2}$ ($\Lambda = \pm 1, \sigma = \pm 1/2$) levels are Zeeman active. In addition, from eq. (10) one sees that the lower J transitions exhibit a greater range of Zeeman tuning, and the requirement for a close match with FIR laser frequency is therefore less stringent. Unfortunately the longest wavelength laser emission attainable in our spectrometer was about 900 μm, limiting the attempt of ClO detection to the $J = 9.5 \leftarrow 8.5$ and higher transitions.

The LMR spectra of ^{35}ClO and ^{37}ClO have been observed at five different FIR laser frequencies as shown in Figures 1 and 2. Identical spectra were recorded by reacting Cl with Cl_2O or O_3, or by reacting O atoms with a large excess of Cl_2. Thus the identity of the absorbing species is certainly ClO. Table II lists all the ClO rotational transitions detected, the FIR laser wavelengths, laser gases, and the laser electric vector polarization with respect to the magnetic field (π = parallel, σ = perpendicular). The assignments were made based on the molecular constants reported previously [17].

For the $J' = 11.5 \leftarrow J'' = 10.5$ π-polarization transition of ^{37}ClO ($^2\Pi_{3/2}$, $v = 0$), a detailed theoretical calculation was carried out.[2] The calculation involves diagonalization of an effective Hamiltonian matrix ($\mathcal{H}_{eff}$) between basis-set wave functions to obtain rotational energies as a function of magnetic field strength. In this study only the $^2\Pi_{3/2}$ wave functions are
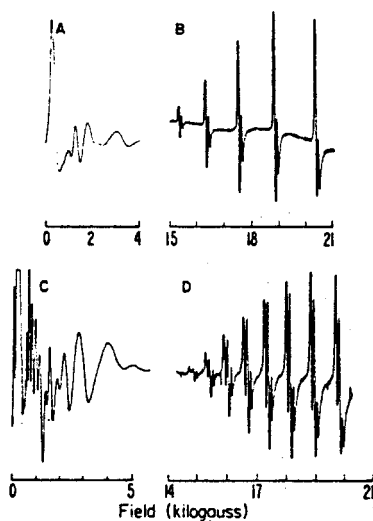
Figure 1. LMR spectra of ClO. A—π spectrum of ^{35}ClO ($J = 14.5 \leftarrow 13.5$) using 556.9 μm CD_3I line; B—σ spectrum of ^{35}ClO ($J = 11.5 \leftarrow 10.5$) using 699.5 μm CH_3OH line; C—same as A, except in σ polarization; D—σ spectrum of ^{37}ClO ($J = 16.5 \rightarrow 17.5$) using 469.1 μm CH_3OH line.

[2] For a complete derivation see [25].
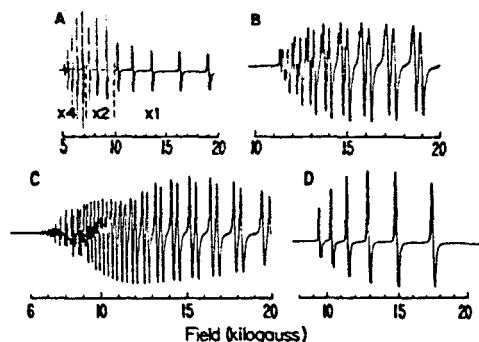
Figure 2.   LMR spectra of ^{37}ClO.   A—σ spectrum of $J = 10.5 \rightarrow 11.5$ transition using 713.1 μm DCOOH line; B—π spectrum of $J = 17.5 \rightarrow 18.5$ transition using 444.4 μm CD$_3$I line; C—same as B, except in σ polarization; D—same as A, except in π polarization.

included in the basis set because ClO is a very good Hund's case (a) type molecule, and the mixing between the $^2\Pi_{3/2}$ and $^2\Pi_{1/2}$ levels is not important ($A \simeq 319$ cm^{-1}).   The Cl nucleus has a spin of $I = 3/2$, and since hyperfine effects produce observable but not completely resolved splittings, nuclear spin effects are included.   Thus the total angular momentum $F = J + I$ and the basis set wave functions are characterized by the following quantum numbers:

$$(11) \qquad \Psi = |\Lambda S\Sigma Im\rangle |\Phi FM_F\rangle$$

where S is the total spin angular momentum quantum number; m is the projection of I on the molecular axis and may have four values, 3/2, 1/2,

TABLE II.   Summary of observed ClO spectra.

Species Detected	$J' \leftarrow J''$	Laser Gas	λ_{laser} (µm)	CO$_2$ Pump Laser Line	Polarization
^{35}ClO	11.5←10.5	CH$_3$OH	699.5	9P34	$\sigma(\Delta M_J = +1)$
^{37}ClO	17.5←16.5	CH$_3$OH	469.1	10R38	$\sigma(\Delta M_J = +1)$
^{35}ClO	14.5←13.5	CD$_3$I	556.9	10P36	σ
^{35}ClO	14.5←13.5	CD$_3$I	556.9	10P36	$\pi(\Delta M_J = 0)$
^{37}ClO	18.5←17.5	CD$_3$I	444.4	9R32	σ
^{37}ClO	18.5←17.5	CD$_3$I	444.4	9R32	π
^{37}ClO	11.5←10.5	DCOOH	713.1	10R34	$\sigma(\Delta M_J = +1)$
^{37}ClO	11.5←10.5	DCOOH	713.1	10R34	$\pi(\Delta M_J = 0)$

−1/2, and −3/2; Φ is the projection quantum number of F on the molecular axis; $\Phi = \Lambda + \Sigma + m$; and M_F is the projection quantum number of F in the direction of the magnetic field. The basis set consists of 32 wave functions corresponding to eight sequential values of F, and each F value generates four hyperfine sublevels corresponding to the four possible values of m.

The $\mathcal{H}_{eff}$ is derived from a complete Hamiltonian, which is essentially the one given by Carrington [24]. Since the basis set contains only $^2\Pi_{3/2}$ wave functions, this Hamiltonian is simplified to a great extent, that is, all terms that mix the $^2\Pi_{3/2}$ ground state with states of different Λ or Σ are neglected. The resulting $\mathcal{H}_{eff}$ is given below, where it has been divided into four parts, spin rotation (sr), hyperfine (hf), quadrupole (Q), and Zeeman (Z):

(12) $\mathcal{H}_{sr} = B[F(F+1) + S(S+1) + I(I+1) - \Phi^2$
$$- \Lambda^2 - \Sigma^2 - m^2 - F_+I_- - F_-I_+] + A\Lambda\Sigma$$

where $F_\pm = F_x \pm iF_y$, A is the spin-orbit coupling constant, and B is the rotational constant.

(13) $$\mathcal{H}_{hf} = am\Lambda + (b+c)m\Sigma$$

where a, b, and c are Frosch and Foley hyperfine constants.

(14) $$\mathcal{H}_Q = \frac{e^2Qq}{4I(2I-1)}[3m^2 - I(I+1)]$$

where e^2Qq is the quadrupole coupling constant.

(15) $$\mathcal{H}_Z = \mu_B H\alpha_{Zz}(\Lambda + g_e\Sigma) + g_I\mu_N H(\alpha_{Zz} + \alpha_{Zx}I_x + \alpha_{Zy}I_y)$$

where α_{Zz}, α_{Zx}, and α_{Zy} are direction cosine matrix elements, g_e is the electron spin g factor, g_I is the nuclear spin g factor, and μ_N is the nuclear magneton.

The matrix elements can be calculated exactly from known relations for the direction cosine matrix elements and ladder operators (see, for example, [26]). Nonzero matrix elements of $\mathcal{H}_{eff}$ result only for diagonal elements and for those basis set functions that are connected by the quantum number changes $\Delta F = 0$ or ± 1 and/or $\Delta\Phi = \Delta m = 0$ or ± 1. A computer program which calculates these matrix elements as a function of F, M_F, and H and diagonalizes the resulting 32 × 32 matrix to yield rotational energies and wave functions has been developed [25].

The program was used to simulate the ^{37}ClO π-polarized, $J = 11.5 \leftarrow 10.5$ spectrum obtained by using the 713.1-μm DCOOH laser line. The appropriate molecular constants for ^{37}ClO are $B = 0.609295$ cm^{-1} [17], $A = -318.7$ cm^{-1} [19], $a + 1/2(b+c) = 3.1305 \times 10^{-3}$ cm^{-1} [21], $e^2Qq = 2.316 \times 10^{-3}$ cm^{-1} [17] and $g_I = 1.7395 \times 10^{-8}$ cm$^{-1}\cdot$G^{-1} [27]. For this transition the energy required for zero-field absorption is ∼14.009 cm^{-1} (Table I). To achieve resonance with the FIR laser energy at ∼14.023 cm^{-1}, this rotational

transition must be Zeeman tuned by an amount equal to ∼0.014 cm^{-1}. The observed spectrum was simulated by calculating the magnetic fields required for resonance with each hyperfine component of a J', $M'_J \leftarrow J''$, M''_J transition. Although the program is written in terms of the quantum numbers F and M_F, the program output is easily interpreted in terms of J and M_J from the strong J dependence of the energies and from the relation $M_J = M_F - M_I$, where M_I is the projection quantum number of I on the laboratory (magnetic field) axis. The results of the calculation are given in Table III. The predicted magnetic field for each hyperfine component is also compared with the observed spectrum in Figure 3. The observed hyperfine structure is not well resolved. Only the transitions at the lower fields show structure on the high-field side of the absorption peaks. However, the observed contours are in qualitative agreement with the predicted hyperfine splittings, and the position of each hyperfine quartet is in excellent agreement with the observations. The relative intensities shown in Figure 3 are obtained by calculating a quantity proportional to the square of the dipole transition moment integral, $\langle \Phi_L | \alpha_{Zz} |$

TABLE III. Results of calculation for the $J' = 11.5 \leftarrow J'' = 10.5$, $\pi(\Delta M_J = 0)$ spectrum of ^{37}ClO.

M_J	$H_{calculated}$ (kG)	$H_{observed}$ (kG)
-10.5	8.398	8.43
	8.370	
	8.412	
	8.510	
-9.5	9.299	9.32
	9.276	
	9.318	
	9.413	
-8.5	10.420	10.44
	10.403	
	10.442	
	10.535	
-7.5	11.855	11.87
	11.844	
	11.884	
	11.971	
-6.5	13.757	13.73
	13.752	
	13.792	
	13.875	
-5.5	16.411	16.34
	16.411	
	16.450	
	16.529	
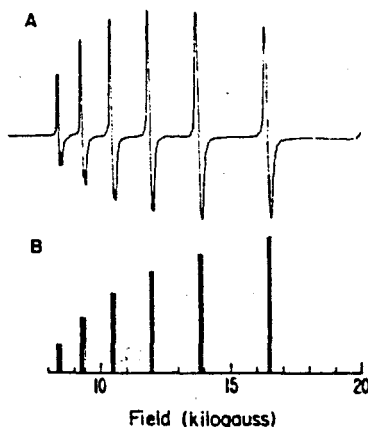
Figure 3. Comparison of the calculated results with the observed π spectrum of ^{37}ClO ($J = 10.5 \rightarrow 11.5$) using the 713.1-$\mu$m DCOOH laser line. A—observed; B—calculated.

$\Phi_l\rangle^2$, where the subscripts u and l refer to the upper and lower states, respectively. The relative intensity comparison between these calculated values and the LMR observations is only qualitative because other factors, such as field homogeneity and the absorption linewidth [28], affect the observed first derivative spectra. However, the overall agreement between the observed and calculated spectra clearly indicates that we are detecting ClO in the $X^2\Pi_{3/2}(v = 0, J = 11.5 \leftarrow 10.5)$ transition.

Kinetic Results

Kinetic Studies of ClO + NO$_2$ + M Reaction

All the kinetic measurements were made under pseudo-first-order conditions ([NO$_2$] $\gg$ [ClO]) such that the NO$_2$ concentration was constant during each measurement of the first-order ClO decay. Under such conditions, the rate expression for reaction (6) is written as

$$(16) \qquad -\bar{v}\frac{d(\ln [ClO])}{dz} = k_M^{III}[NO_2][M] = k^{II}[NO_2] = k^{I}$$

where $\bar{v}$ is the average flow velocity, z is the distance from the end of the movable injector to the detection volume, [M] is the concentration of the third body, and k^I, k^{II}, and k^{III} are the effective first-order, second-order, and third-order rate constants, respectively.

A set of typical ClO decay plots is shown in Figure 4. Each measurement was made by varying the reaction distance z by 20–30 cm. The decay of [ClO] in the measurements was greater than a factor of 1.5, but less than
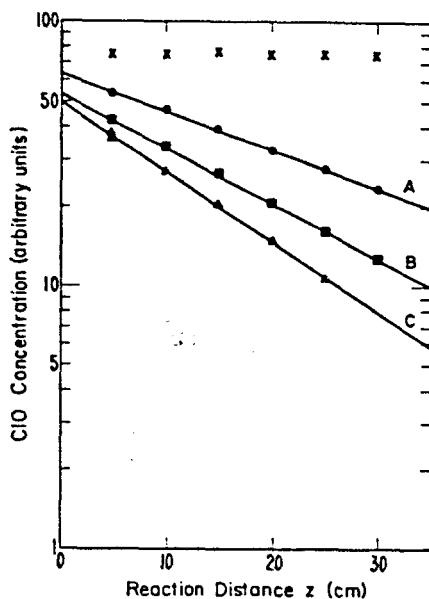
Figure 4. Pseudo-first-order decay plot for ClO + NO$_2$ + O$_2$ reaction. $T = 298$ K, $P_t = 3.09$ torr, $\bar{v} = 480$ cm/s, [O$_2$] = 8.46 × 10^{16} molec/cm^3, [He] = 1.44 × 10^{16} molec/cm^3. A—[NO$_2$] = 8.04 × 10^{14} molec/cm^3; B—[NO$_2$] = 1.14 × 10^{15} molec/cm^3; C—[NO$_2$] = 1.50 × 10^{15} molec/cm^3. The × symbols are the ClO blank measurements showing negligible ClO wall loss, [NO$_2$] = 0.

a factor of 15. The slope of the semilogarithmic plot multiplied by $\bar{v}$ gives the uncorrected first-order rate constant, k_0^I (in s^{-1}). The rate constant was corrected for axial diffusion[3]:

$$(17) \qquad k^I = k_0^I(1 + Dk_0^I/\bar{v}^2)$$

where D is the diffusion coefficient in cm^2/s. The ClO diffusion coefficients were estimated as $490(T/300)^{1.7}P^{-1}$ torr·cm^2/s (P in torr) in He and $130(T/300)^{1.7}P^{-1}$ in N$_2$ and O$_2$. The axial diffusion correction was small, generally less than 6%.

The × symbols near the top of Figure 4 indicate the ClO concentration measured with no NO$_2$ added to the flow system. The near zero change in [ClO] at $T > 250$ K demonstrates that the ClO loss on the flow tube surface is negligible, $k_w < 0.1$ s^{-1}, and that there are no other reactions of ClO.

Figure 5 shows a plot of k^I versus [NO$_2$] for the ClO + NO$_2$ + O$_2$ reaction. The results obtained from Figure 4, lines A–C, are marked A, B, and C, respectively. At each temperature [NO$_2$] was varied while the rest of the experimental conditions remained unchanged. The excellent linearity and zero intercept of this plot show that the equation $k^I = k^{II}$ [NO$_2$] is valid,

---

[3] The axial diffusion correction is given in [29a]; the diffusion coefficients are estimates based on data given in [29b].
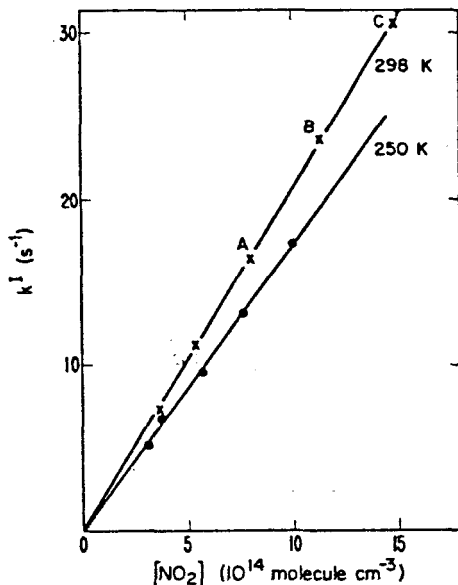
Figure 5.   Plot of k^I versus [NO$_2$] for ClO + NO$_2$ + O$_2$ reaction. $\times$—T = 298 K, P_t = 3.09 torr, slope = 2.04 $\times$ 10^{-14} cm^3/molec·s; $\bullet$—T = 250 K, P_t = 1.24 torr, slope = 1.71 $\times$ 10^{-14} cm^3/molec·s. [NO$_2$] at this temperature has been corrected for dimerization. The results from Figure 4 are marked A, B, and C, respectively.

and the slope gives k^{II}. Some k^{II} measurements in this study were obtained by simply dividing the measured k^I value by [NO$_2$].

A plot of k^{II} versus [M] (total gas density) at 250 and 298 K using He or O$_2$ as a carrier gas is shown in Figure 6. The data shown in Figure 5 for T = 298 and 250 K are indicated by A and B. The linearity of this plot demonstrates that the reaction is third order at pressures below 6 torr. For
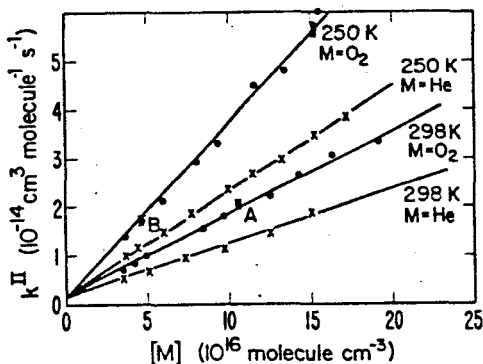
Figure 6.   Plot of k^{II} versus [M] for the ClO + NO$_2$ + M reactions at 250 and 298 K. $\bullet$—M = O$_2$; $\times$—M = He. The data shown in Figure 5 are indicated by A and B.

experiments using He as the third body, the slope gives k_{He}^{III} directly, because the concentrations of other species such as NO_2, O_2, and Cl_2 is negligible. However, for experiments using N_2 or O_2 as the third body the amount of He carrier added through the microwave discharge (ClO source) and the ozone reservoir comprises up to 30% of the gas mixture in the flow tube at low pressures. To derive accurate k_M^{III} values for various third bodies, a linear least-square fit of the data to the expression

(18) $$k^{II} = k_w^{II} + k_{He}^{III}[He] + k_{O_2}^{III}[O_2] + k_{N_2}^{III}[N_2]$$

was carried out by computer. The intercept in the k^{II} versus [M] plot, k_w^{II}, is a pressure-independent heterogeneous contribution to k^{II}, which can be taken as the second-order rate constant for the ClO + NO_2 reaction with the stabilization by wall collisions. Thus for a simultaneous fit, the k_w^{II} value is constrained to be the same for different carrier gases at the same temperature. The magnitude of k_w^{II} is relatively small, $(0.5-2.1) \times 10^{-15}$ cm^3/molec·s, and varies with different wall conditions and temperatures. Therefore experimental data obtained at different times with different wall conditions were grouped separately, as shown in Table IV.

In Table IV, the experimental conditions, k_w^{II}, and k_M^{III} values for N_2 at 297 K and for He and O_2 at six temperatures ranging from 250 to 416 K are summarized. The listed uncertainties for k_w^{II} and k^{III} are one standard deviation of the coefficients derived from the fits of the experimental data to eq. (18). At room temperature k_{He}^{III} was measured as (1.02 ± 0.02), (1.06 ± 0.02), and (1.07 ± 0.02) × 10^{-31} cm^6/molec²·s at three different times with

TABLE IV. Data summary for ClO + NO2 + M reaction.

T(°K)	M	No. Exp.	P_M (torr)	P_{He} (torr)	[NO2] (10^{15} molecule cm⁻³)	k_M^{III} (10^{-31} cm⁶ molecule⁻² s⁻¹)	k_w^{II} (10^{-15} cm³ molecule⁻¹ s⁻¹)
298	He	37	0.91–6.60	0.91–6.60	0.50–3.75	1.02±0.02	2.1±0.3
	N₂	14	0.67–3.70	0.12–0.48	0.94–1.86	2.06±0.06	
298	He	6	1.10–5.92	1.10–5.92	0.37–2.08	1.06±0.02	1.5±0.2
	O₂	11	0.56–5.57	0.26–0.47	0.43–1.68	1.85±0.02	
296	He	18	0.86–4.88	0.86–4.88	0.65–2.34	1.07±0.03	1.9±0.2
	O₂	14	0.96–4.17	0.25–0.38	0.53–1.81	1.88±0.03	
	N₂	8	0.87–4.71	0.24–0.33	0.40–1.23	2.12±0.03	
250	He	9	0.97–4.46	0.97–4.46	0.38–0.83	2.26±0.07[a]	0.7±0.1
	O₂	17	0.71–4.53	0.21–0.29	0.19–1.04	3.86±0.06[a]	
272	He	8	1.13–4.47	1.13–4.47	0.26–0.80	1.50±0.06	1.4±0.6
	O₂	8	0.72–4.23	0.19–0.23	0.25–0.67	2.73±0.06	
342	He	9	0.95–4.46	0.95–4.46	0.80–1.72	0.72±0.02	0.5±0.1
	O₂	10	0.57–4.16	0.21–0.34	0.92–1.69	1.16±0.02	
387	He	8	1.03–3.97	1.03–3.97	1.18–1.82	0.46±0.03	0.9±0.2
	O₂	10	0.24–0.29	0.24–0.29	1.48–1.76	0.74±0.03	
416	O₂	7	0.71–3.58	0.31–0.40	1.33–1.85	0.58±0.03[b]	0.3±0.1

[a] Measured with correction for NO_2 dimerization. Without correction, k_{He}^{III} and $k_{O_2}^{III}$ were 2.17 and 3.69 × 10^{-31} cm^6/molec²·s, respectively.[2] See text.

[b] Assuming k_{He}^{III} = 3.8 × 10^{-32} cm^6/molec²·s. See text.

excellent consistency. Thus an average value of 1.05×10^{-31} cm^6/molec^2·s is obtained for the ClO + NO$_2$ + He reaction at room temperature. Similarly the room temperature values of 1.87×10^{-31} and 2.09×10^{-31} cm^6/molec^2·s are obtained for M = O$_2$ and M = N$_2$, respectively.

At 416 K the ClO + NO$_2$ + He reaction was too slow to be measured. The data for M = O$_2$ at this temperature were corrected for the small contribution from M = He using $k_{He}^{III} = 3.8 \times 10^{-32}$ cm^6/molec^2·s obtained by extrapolating the lower temperature data.

In Figure 7 the data for k_{He}^{III} and $k_{O_2}^{III}$ are plotted as a function of $1/T$. The least-square fits gave $k_{He}^{III} = (2.79 \pm 0.38) \times 10^{-33} \exp[(1087 \pm 41)/T]$ and $k_{O_2}^{III} = (3.48 \pm 0.22) \times 10^{-33} \exp[(1183 \pm 19)/T]$ cm^6/molec^2·s, where the error limits are one standard deviation limits on the coefficients.

As mentioned earlier, the concentration of N$_2$O$_4$ becomes significant only at the lowest temperatures. An attempt was made to measure the rate constant for the reaction of ClO with N$_2$O$_4$. A special double port movable inlet was constructed. One port was designed to maximize the N$_2$O$_4$ concentration injected into the flow tube. It had a short ($\approx$1.5 cm) length of 0.09-mm inside diameter capillary attached to the end of a 14-mm inside diameter $\times$ 10-cm length bulb. This constriction caused a high pressure ($\sim$40 torr) to develop inside the inlet and therefore enhanced the NO$_2$ dimerization. The pressure in the inlet was measured and the fractional dimerization was calculated using the equilibrium constant [15]. At 255
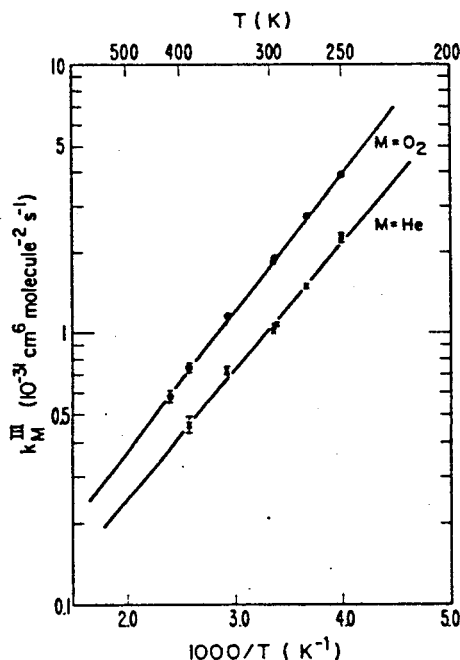
Figure 7.   Arrhenius plot of $k_{O_2}^{III}$ and k_{He}^{III} for ClO + NO$_2$ + M reaction.

K the N_2O_4 flow rate was typically 70–80% of the total flow rate (N_2O_4 + NO_2). Equilibrium was assured by the long residence time in the cooled inlet tube (~7 s). The second port was designed for minimum dimerization, with low pressure and a short residence time. For these measurements the ClO was added to the carrier gas upstream from the reaction zone. When a mixture of about 75% N_2O_4 and 25% NO_2 was reacted with ClO, the observed ClO loss rate was significantly less (~1/2) than when the same flow rate was added through the second injector port as monomers. From this observation we conclude that small amounts of N_2O_4 do not interfere with the ClO + NO_2 kinetic measurements. The N_2O_4 is probably not dissociated significantly in the flow tube at 255 K and pressures of a few torr. If that is true, then $k(\text{ClO} + N_2O_4) \simeq 2 \times 10^{-14}$ cm³/molec·s.

Kinetic Studies of ClO + NO → Cl + NO₂ Reaction

A typical ClO decay plot is shown in Figure 8. In these measurements the reaction distance z was varied by 15–30 cm. The ClO decay with no NO added (× symbols at the top of Figure 8) also indicated negligible wall loss. The axial diffusion correction was applied and was less than 8% at 209 K and 3% at 393 K.

Figure 9 shows a plot of k^1 as a function of [NO] for data at 393, 296, and 202 K. At room temperature, some measurements (indicated ▲ on Figure
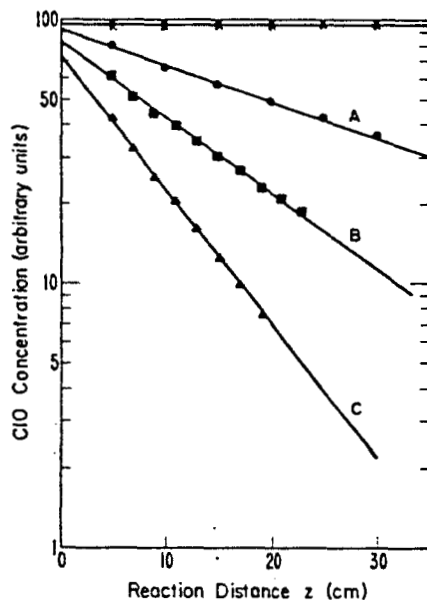
Figure 8. Pseudo-first-order decay plot for ClO + NO reaction. T = 393 K, P_t = 1.91 torr, $\bar{v}$ = 2210 cm/s. A—[NO] = 5.27 × 10¹² molec/cm³; B—[NO] = 1.19 × 10¹³ molec/cm³; C—[NO] = 2.01 × 10¹³ molec/cm³. The × symbols are the ClO measurements showing negligible ClO wall loss, [NO] = 0.
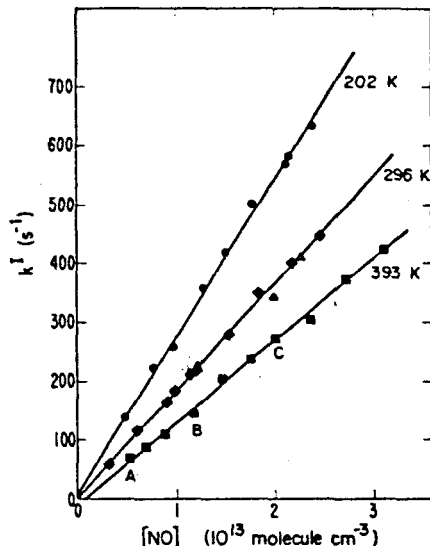
Figure 9. Plot of k^I versus [NO] at 202, 296, and 393 K for ClO + NO reaction. At 296 K. ♦—NO through the movable injector; ▲—ClO through the movable injector. A, B, and C indicate data from Figure 8.

9) were performed by adding ClO through the movable inlet and adding NO with the carrier gas. No difference in rate constant was observed. No pressure dependence was observed over the range of 1–3 torr. The data for k^I versus [NO] at each temperature were fitted with a least-squares program to a straight line. The slope k^{II}, intercept, and experimental conditions at five temperatures ranging from 202 to 393 K are summarized in Table V. At room temperature the rate constants were measured as 1.66, 1.84, and 1.84 × 10^{-11} cm³/molec·s at three different times. These give an average value of 1.78 × 10^{-11} cm³/molec·s.
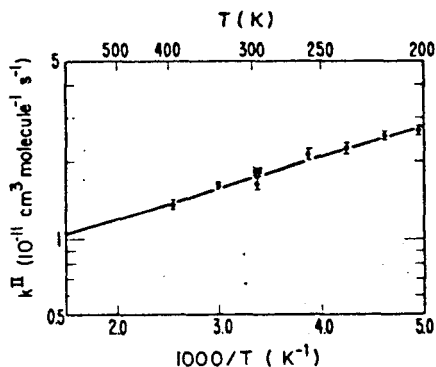
Figure 10. Arrhenius plot for ClO + NO → Cl + NO₂ reaction rate constant data.

TABLE V. Data summary for ClO + NO reaction.

T(°K)	No. Exp	P_t (torr)	[NO] (10^{13} molecule cm^{-3})	k (10^{-11} cm^3 molecule^{-1} s^{-1})	Intercept (s^{-1})
295	10	0.94-2.56	0.33-2.47	1.84±0.03	0±4
296	17	1.05-3.10	0.82-2.97	1.66±0.04	13±3
297	8	1.11	0.41-2.10	1.84±0.03	10±5
202	10	1.04-1.99	0.49-2.39	2.64±0.06	14±9
217	9	1.01-1.94	0.33-2.40	2.52±0.05	13±7
236	9	1.04-1.95	0.43-2.30	2.25±0.06	7±8
254	10	1.11-1.12	0.92-3.19	2.13±0.05	-13±12
333	10	1.01-2.61	0.36-2.77	1.63±0.02	-1±4
393	10	1.91-2.77	0.53-3.10	1.39±0.03	-11±6

The measured rate constants are plotted versus $1/T$ in Figure 10. A least-squares fit to the Arrhenius expression gives $k_3 = (7.13 \pm 0.48) \times 10^{-12}$ exp $[(271 \pm 18)/T]$ cm^3/molec·s, where the error limits represent one standard deviation.

Discussion

The measurements of $k(\text{ClO} + \text{NO}_2 + \text{M})$ are summarized with the work from other laboratories in Table VI. The error limits have been increased to allow for systematic errors. Our M = He measurement is about in the middle of the values obtained by Leu et al. [8] and Zahniser et al. [10] and agrees well with the 297 K value reported by Birks et al. [9]. The range of these measurements at room temperature is about ±15%. For M = N$_2$ we measured k only at 297 K. Our result is higher than all of the published values. The maximum discrepancy is 38% compared to Zahniser et al. Although the error bars on these measurements nearly overlap, this dif-

TABLE VI. Comparison of results for ClO + NO$_2$ + M reaction.

M	Arrhenius Form	T (K)	k(298K) (10^{-31} cm^6 molecule^{-2} s^{-1})	P (torr)	Technique[a]	Reference
He	$(2.8\pm0.6)\times10^{-33}$ exp[(1090±80)/T]	250-387	1.05±0.15	0.67-6.60	DF-LMR	This Work
	$(3.54\pm0.06)\times10^{-33}$ exp (950/T)	250-365	0.83±0.12	1.1 -6.5	DF-RF	Zahniser et al.[10]
	$(2.66\pm0.35)\times10^{-33}$ exp[(1140±40)/T]	248-417	1.20±0.05	1-9	DF-MS	Leu et al.[8]
	-	297	0.96±0.03	2.5 -5.0	DF-MS	Birks et al.[9]
N$_2$	-	297	2.09±0.30	0.67-3.70	DF-LMR	This work
	-	297	1.52±0.23	2-4.1	DF-RF	Zahniser et al.[10]
	$(3.69\pm0.24)\times10^{-33}$ exp[(1150±20)/T]	298-417	1.72±0.17	1-6	DF-MS	Leu et al.[8]
	$(4.40\pm0.66)\times10^{-33}$ exp[(1087±70)/T]	250-356	1.85±0.05	1.5-4.5	DF-MS	Birks et al.[9]
	$(4.3\pm1.2)\times10^{-33}$ exp[(1085±86)/T]	274-339	1.66	50	MA	Cox and Lewis[30]
			1.5 ±0.12	20	FP-A	Molina et al.[34]
O$_2$	$(3.5\pm0.6)\times10^{-33}$ exp[(1180±80)/T]	250-416	1.86±0.28	0.56-5.57	DF-LMR	This work
Ar	-	298	1.15±0.10	1-4	DF-MS	Leu et al.[8]

[a] DF—discharge flow; LMR—laser magnetic resonance; RF—resonance fluorescence; MS—mass spectrometry; MA—modulated absorption; FP-A—flash photolysis ultraviolet absorption.

ference is larger than is normally found. This work is the only reported measurement with $M = O_2$. We can compare this result with the earlier work on the basis of the temperature dependence, which agrees very well with previous measurements in He and N_2.

Cox and Lewis [30] have reported the most extensive pressure dependence study of reaction (6). They measured the rate constant in N_2 over the range of 25–612 torr using modulated photolysis with ultraviolet absorption detection of ClO. Their data connect reasonably well with the low-pressure data, as seen in Table VI. They report some falloff at pressures greater than 50 torr.

Molina et al. [34] have measured k_6 at 298 K in 20 and 100 torr N_2 using a flash-photolysis ultraviolet absorption technique. Their result using a Cl_2O source of ClO agrees reasonably well with the others.

The product of the termolecular reaction of ClO and NO_2 was not quantitatively observed here or in most of the previous studies [8–10]. It has been suggested [31–34] that more than one isomer of $ClNO_3$ may be formed. The possibilities include the following

(6a) $ClO + NO_2 + M \rightarrow ClONO_2 + M$

(6b) $\rightarrow ClOONO + M$

(6c) $\rightarrow OClNO_2 + M$

(6d) $\rightarrow OClONO + M$
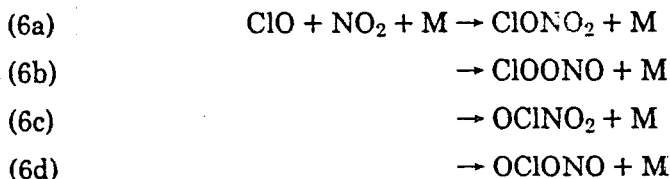
The studies of the thermal decomposition of $ClONO_2$ [31] and the isotopic exchange reaction between $ClONO_2$ and $^{15}NO_2$ by Knauth and co-workers [32], when combined with the equilibrium constant for $ClONO_2$ formation, lead to a value of $k_{N_2}^{III}$ that is about 30% of the values listed in Table VI. It is not clear that this difference is significant due to uncertainties in the thermochemical data. Chang et al. [33] suggested, on the basis of a recombination theory calculation, that if the isomer ClOONO is formed along with $ClONO_2$, the discrepancy between the forward and reverse rate constants of $ClNO_3$ can be resolved. Recently, in a flash-photolysis experiment, Molina et al. [34] have observed different rates of removal of ClO depending upon the ClO precursor (Cl_2O or OClO). They proposed that an OClONO isomer is formed and takes part in a secondary reaction. Using infrared absorption spectroscopy, they also found that the amount of $ClONO_2$ produced was only about one third of the amount of ClO removed. Thus it is probable that more than one product is formed in this reaction. This conclusion has a very important implication to atmospheric chemistry because the identity of the product molecule determines the photolysis rates and products and hence the effect of the $ClO + NO_2 + M$ reaction. The large rate constant for the reaction makes it a potentially important process for ClO in the stratosphere. Therefore the reaction products must be determined and evaluated.

The measurement using O_2 as a carrier gas was carried out to investigate the possiblity of a reaction rate enhancement by O_2. The reaction of O_2 with ClO to form $OClO_2$,

(7) $ClO + O_2 + M \rightleftharpoons OClO_2 + M$

may be possible,[4] although no information on the reaction rate is available. If reaction (7) is sufficiently fast and followed by the reaction

(19) $OClO_2 + NO_2 \rightarrow ClNO_3 + O_2$

the rate of $ClNO_3$ formation could be enhanced in oxygen. Assuming a steady state of $[ClO_3]$, the rate constant enhancement is $k_{19}k_7[O_2]/(k_{-7}[M] + k_{19}[NO_2])$, where k_{-7} is the back-reaction rate constant for reaction (7). In the present experiment the variation of $[O_2]$ and $[NO_2]$ was not large enough to observe a significant enhancement due to this mechanism.

The measured relative third-body efficiencies of 1.0:1.8:2.0 for He, O_2, and N_2, respectively, in $ClO + NO_2 + M$ reaction can be compared with those obtained for the similar reaction

(20) $HO_2 + NO_2 + M \rightarrow HOONO_2 + M$

by Howard [36], namely, 1.0:1.5:2.1. Although the O_2 third-body efficiency measured in this study for reaction (6) is slightly higher than that of reaction (20), the difference is too small to be considered significant.

The activation energy of $k_{O_2}^{III}$, (1180 ± 80), is slightly higher than that of k_{He}^{III}, (1090 ± 80). Although the difference may be due to the experimental uncertainties, the possibility remains that this is an indication of a different mechanism for $ClO + NO_2$ reaction in O_2. We plan to extend these measurements to higher pressures as a further test for a mechanism involving $OClO_2$.

The measurements of the $ClO + NO$ rate constant k_3 are summarized

TABLE VII.   Comparison of rate constant measurements for $ClO + NO \rightarrow Cl + NO_2$ reaction.

Temp. Range (K)	Arrhenius Form $(cm^3 molecule^{-1}s^{-1})$	$k(298K)$ $(10^{-11} cm^3 molecule^{-1}s^{-1})$	Method[a]	Reference
202-393	$(7.1\pm1.4)\times10^{-12}exp[(270\pm50)/T]$	1.7±0.27	DF-LMR	This work
298	-	1.7 ±0.2	DF-MS	Clyne and Watson[3]
230-295	$(1.13\pm0.14)\times10^{-11}exp[(200\pm30)/T]^b$	2.2 ±0.4[b]	DF-RF	Zahniser and Kaufman[4]
227-415	$(5.72\pm0.18)\times10^{-12}exp[(296\pm20)/T]$	1.53±0.11	DF-MS	Lau and DeMore[5]
298	-	1.54±0.16	DF-MS	Clyne and MacRobert[6]
298	-	1.75±0.15	DF-MS	Ray and Watson[7]

[a] DF—discharge flow; LMR—laser magnetic resonance; MS—mass spectrometry; RF—resonance fluorescence.

[b] Based on a rate constant ratio measurement as described in text.

[4] Prasad [35] also recently discussed some possible implications of $OClO_2$ in stratospheric chemistry.

in Table VII. Our room temperature measurement is in excellent agreement with those of Clyne and Watson [3] and Ray and Watson [7] and in good agreement with the other measurements. The temperature dependence is very close to the result of Leu and DeMore [5], although their rate constants fall about 15% below ours. The temperature dependence given by Zahniser and Kaufman [4] is also in good agreement, but their values fall somewhat higher than ours. The k_3 given in Table VII for Zahniser and Kaufman is based on their measurement of the ratio of k_3 to $k(Cl + O_3)$ and their value for $k(Cl + O_3)$.

In conclusion, we find that the LMR technique can be used to detect ClO radicals with sufficient sensitivity to allow pseudo-first-order kinetic studies in a flow-tube reactor. This method offers the advantages of positive spectroscopic identification of the ClO with no interference from product species or from problems encountered with indirect measurement methods.

Acknowledgment

Bibliography

[1] F. S. Rowland and M. J. Molina, *Rev. Geophys. Space Phys.*, 13, 1 (1975).

[2] As described later, several different isomers of $ClNO_3$ are possible. The formula $ClNO_3$ as it is used here is not meant to imply any particular isomer, only the empirical formula of the product of reaction (6).

[3] M. A. A. Clyne and R. T. Watson, *J. Chem. Soc., Faraday Trans. I*, 70, 2250 (1974).

[4] M. S. Zahniser and F. Kaufman, *J. Chem. Phys.*, 66, 3673 (1977).

[5] M. T. Leu and W. B. DeMore, *J. Phys. Chem.*, 82, 2049 (1978).

[6] M. A. A. Clyne and A. J. MacRobert, *Int. J. Chem. Kinet.*, 12, 79 (1980).

[7] G. W. Ray and R. T. Watson, 14th Informal Conf. on Photochemistry, Newport Beach, CA, 1980.

[8] M. T. Leu, C. L. Lin, and W. B. DeMore, *J. Phys. Chem.*, 81, 190 (1977).

[9] J. W. Birks, B. Shoemaker, T. J. Leck, R. A. Borders, and L. J. Hart, *J. Chem. Phys.*, 66, 4591 (1977).

[10] M. S. Zahniser, J. S. Chang, and F. Kaufman, *J. Chem. Phys.*, 67, 997 (1977).

[11] C. J. Howard and K. M. Evenson, *J. Chem. Phys.*, 61, 1943 (1974).

[12] R. M. Stimpfle, R. A. Perry, and C. J. Howard, *J. Chem. Phys.*, 71, 5183 (1979).

[13] R. T. Watson, *J. Phys. Chem. Ref. Data*, 6, 871 (1977).

[14] R. J. Nordstrom and W. H. Chan, *J. Phys. Chem.*, 80, 847 (1976).

[15] D. R. Stull and H. Prophet, Eds., "JANAF Thermochemical Tables," Nat. Bur. Stand., Washington, DC, including revised tables issued through 1979.

[16] W. B. DeMore and O. Raper, *J. Phys. Chem.*, 68, 412 (1964).

[17] R. K. Kakar, E. A. Cohen, and M. Geller, *J. Mol. Spectrosc.*, 70, 243 (1978).

[18] T. Amano and E. Hirota, *J. Mol. Spectrosc.*, 66, 185 (1977).

[19] U. Uehara, M. Tanimoto, and Y. Morino, *Mol. Phys.*, 22, 799 (1971).

[20] A. Carrington, P. N. Dyer, and D. H. Levy, *J. Chem. Phys.*, 47, 1756 (1967).
[21] T. Amano, S. Saito, E. Hirota, Y. Morino, D. R. Johnson, and F. X. Powell, *J. Mol. Specrosc.*, 30, 275 (1969).
[22] J. A. Coxon, W. E. Jones, and E. G. Skolnik, *Can. J. Phys.*, 54, 1043 (1976).
[23] R. T. Menzies, J. S. Margolis, E. D. Hinkley, and R. A. Toth, *Appl. Opt.*, 16, 523 (1977).
[24] A. Carrington, "Microwave Spectroscopy of Free Radicals," Academic, New York, 1974, p. 192.
[25] R. M. Stimpfle, Ph.D. dissertation, Department of Chemistry, University of Colorado, Boulder, CO, 1979, chap. 2.
[26] J. T. Hougen, "The Calculation of Rotational Energy Levels and Rotational Line Intensities in Diatomic Molecules," NBS Monograph 115, June 1970, p. 31.
[27] C. H. Townes and A. L. Schawlow, "Microwave Spectroscopy," McGraw-Hill, New York, 1955, p. 644.
[28] J. T. Hougen, *J. Mol. Spectrosc.*, 54, 477 (1975).
[29] (a) F. Kaufman, *Prog. React. Kinet.*, 1, 3 (1961); (b) T. R. Marrero and E. A. Mason, *J. Phys. Chem. Ref. Data*, 1, 3 (1972).
[30] R. A. Cox and R. Lewis, *J. Chem. Soc., Faraday Trans. I*, 75, 2649 (1979).
[31] H. D. Knauth, *Ber. Bunsenges. Phys. Chem.*, 82, 212 (1978).
[32] G. Schönle, H. D. Knauth, and R. N. Schindler, *J. Phys. Chem.*, 83, 3297 (1979).
[33] J. S. Chang, A. C. Baldwin, and D. M. Golden, *J. Chem. Phys.*, 71, 2021 (1979).
[34] M. J. Molina, L. T. Molina, and T. Ishiwata, *J. Phys. Chem.*, 84, 3100 (1980).
[35] S. S. Prasad, *Nature*, 285, 152 (1980).
[36] C. J. Howard, *J. Chem. Phys.*, 67, 5258 (1977).